Phase space analysis of a dynamical model for the subcritical transition to turbulence in plane Couette flow

O. Dauchot[1,a] and N. Vioujard[2]

[1] SPEC, CEA Saclay, 91191 Gif-sur-Yvette, France
[2] École Nationale des Ponts et Chaussées, 77455 Marne-la-Vallée, France

Abstract. Various experiments have outlined generic properties of the subcritical transition to turbulence in plane Couette flow. A low order model of a self-sustaining process has been derived by Waleffe [11] from the Navier-Stokes equations for a sinusoidal shear flow. This paper investigates the weakly non-linear properties and the phase space analysis of this model, including the dependence on the model parameters. It is shown that the asymptotic dynamics essentially reduces to a bidimensional manifold, that many trajectories exhibit long transients, and that a statistical description of the nonlinear response to finite amplitude perturbations is needed in order to recover the bifurcation diagram from an experimental point of view. Comparison with recent experimental results obtained in the plane Couette flow finally outlines the relevance of this kind of approach.

PACS. 05.45.-a Nonlinear dynamics and nonlinear dynamical systems – 47.20.Ft Instability of shear flows – 47.20.Ky Non linearity (including bifurcation theory)

1 Introduction

For the past few years a number of experimental and numerical studies have lead to the formulation of several characteristic features of the transition to turbulence in plane Couette flow; the flow driven by two walls moving in opposite direction at the same speed, a prototype flow for the subcritical transition to turbulence.

(1) Subcriticality: Whereas the laminar velocity profile is stable to infinitesimal perturbations for all Reynolds number, finite amplitude perturbations may trigger an abrupt transition for $R > R_g$, leading to the observation of a sustained disordered flow [2].

(2) Spatio-temporal intermittency: This disordered flow is made of turbulent domains, which move, grow, decay, split and merge leading to spatio-temporal intermittency, that is a coexistence dynamics in which active/turbulent regions may invade absorbing/laminar ones where turbulence cannot emerge spontaneously [3].

(3) Meta-stability: There exists a range of Reynolds number $R_u < R < R_g$ for which the spatio-temporal intermittent regime is sustained for long times but not asymptotically, whatever the perturbation [4].

(4) Transients: When the perturbation does not lead to the sustained spatio-temporally intermittent regime, it may either relax rapidly or exhibit long-lived transients [5]. These transients occur for $R_u < R < R_g$, but

[a] e-mail: `dauchot@spec.saclay.cea.fr`

also for $R > R_g$, when the perturbation is not strong enough.

(5) Strong dependence on the perturbation: The system response to the finite amplitude triggering can be very dispersed. For a given Reynolds number and almost identical disturbances, the flow may either relax to the laminar flow rapidly or transiently, or become a sustained disordered flow [5].

(6) Unstable states: Various unstable finite amplitude solutions made of streamwise vortices and streaks coexist for a transitional Reynolds number. The turbulent state is reminiscent of these states [6–9].

Various dynamical models have attempted to render these essential behaviors. A first set of models (see [10] for a review) dealt with the existence of transient growths and their role in the transitional process. These models have been shown to violate basic nonlinear properties of the Navier-Stokes operator [11], and consequently to be useless for predicting global features. On the basis of a full phase space analysis of a very much simplified model that mimics Navier-Stokes equations, Dauchot and Manneville [12] have stressed the importance of considering global dynamical properties when looking for actual stability boundaries. On the other hand their model is obviously not realistic enough to describe features such as those listed above. More realistic is Schmiegel and Eckhardt's model [13], a 19 dimensional Galerkin approximation to a parallel shear flow, stable for all Reynolds number. This model successfully describes the existence
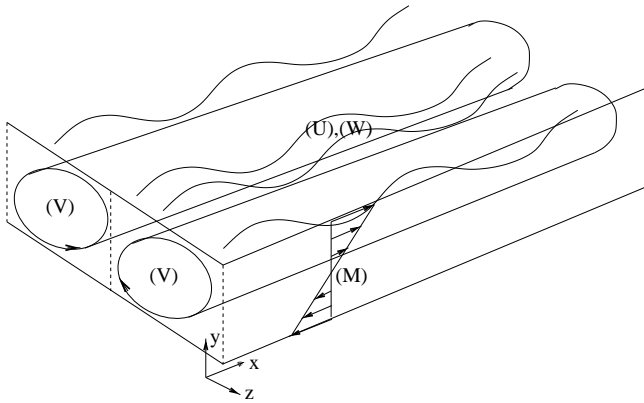
Fig. 1. Schematic drawing of the main shear (M), the stream-wise vortices (V), the streaks (U) and their streamwise oscillations (W) involved in the sustained turbulent process.
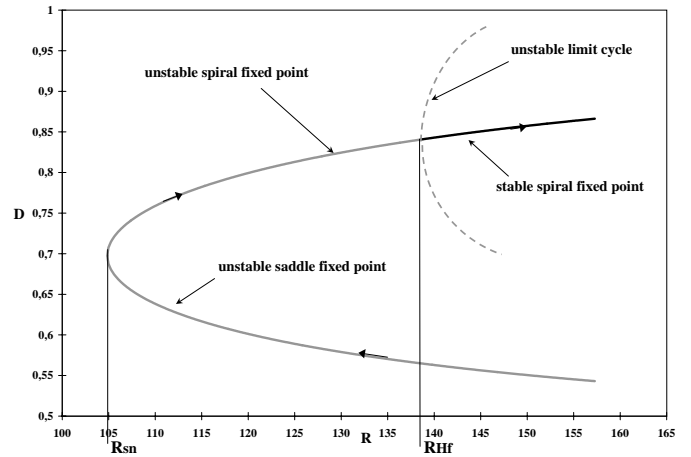

Fig. 2. Bifurcation diagram for $\alpha = 1.303$ and $\gamma = 2.280$. Grey lines are unstable states and dark lines are stable states. The limit cycle shown as a dotted line has not been computed and is plotted for the purpose of the illustration only.

of additional unstable states as well as long lived transients together with their lifetime dispersion. On the other hand it is already too complex to allow a full phase space description and/or to give a precise physical meaning to each mode. Waleffe [1] has derived from the Navier-stokes equation a four dimensional model of the self-sustained turbulence mechanism proposed by Hamilton Kim and Waleffe [14]. This derivation implies such a severe truncation that the adequacy of the model with real hydrodynamics is not guaranteed.

In this paper, we take advantage of the low dimensionality of Waleffe's model to perform its full phase space analysis, in order to evaluate to what extent a statistical analysis of the asymptotic dynamics describes the temporal nonlinear response of the plane Couette flow to finite amplitude disturbances.

2 The model

Hamilton *et al.*'s approach was to extract the mechanisms that maintain turbulence. Guided by a large amount of previous work, (see [14] for a review) they identified a self-sustaining process. First, weak streamwise rolls, (V), redistribute the streamwise momentum of the main flow, (M), and create large spanwise fluctuations in the streamwise velocity, the so-called streaks, (U). Spanwise inflections then drive an instability in which a three-dimensional disturbance develops, (W). Through nonlinear coupling this re-energizes the initial streamwise rolls. The four dimensional model of this process, derived by Waleffe, reads:

$$\frac{\mathrm{d}M}{\mathrm{d}t} + \frac{\kappa_m^2}{R}M = \sigma_m W^2 - \sigma_u UV + \frac{\kappa_m^2}{R},$$

$$\frac{\mathrm{d}U}{\mathrm{d}t} + \frac{\kappa_u^2}{R}U = -\sigma_w W^2 + \sigma_u MV,$$

$$\frac{\mathrm{d}V}{\mathrm{d}t} + \frac{\kappa_v^2}{R}V = \sigma_v W^2,$$

$$\frac{\mathrm{d}W}{\mathrm{d}t} + \frac{\kappa_w^2}{R}W = \sigma_w UW - \sigma_m MW - \sigma_v VW.$$

In these equations, M, U, V and W must be understood to be the amplitude of Galerkin modes with specific spa-

tial structures. More specifically, M is the amplitude of the mean flow, U corresponds to the streaks, V to the streamwise rolls and W gathers several contributions to the instability modes of the streaks. The coefficients depend on (α, β, γ) [1], where γ is the wave number of the streamwise rolls in the spanwise direction, α is the wave number of the streak instability mode in the streamwise direction and $\beta = \pi/2$ is constant. (α, β, γ) verify condition (1): $\gamma^2 > \alpha^2 + \beta^2$.

Waleffe [1] derived the following properties of the model. In addition to the so-called "laminar" trivial fixed point $(M = 1, U = 0, V = 0, W = 0)$, there are two other fixed points which emerge "from nothing" at finite distance from the basic state for $R = R_{\mathrm{sn}}$ (saddle node bifurcation). The smallest Reynolds number at which the saddle-node bifurcation takes place is $R_{\mathrm{sn}} = 104.849$ for $\alpha = 1.303$ and $\gamma = 2.280$. The laminar fixed point remains linearly stable for all values of Reynolds number. The linear stability analysis of the two non-trivial fixed points indicates that one of them is always unstable (the so-called lower branch), whereas the other (the upper branch) may be unstable or stable depending on the set (α, γ, R). For $\alpha = 1.303$ and $\gamma = 2.280$, the upper branch fixed point is an unstable node, which rapidly turns into an unstable spiral at $R = 104.94$ and finally becomes stable through a subcritical Hopf bifurcation at $R = R_{\mathrm{Hf}} = 138.06$. Then unstable spiral fixed point bifurcates into an unstable limit cycle surrounding the newly stable spiral. Figure 2 displays the bifurcation diagram, namely the Euclidean distance D separating the non-trivial states from the basic state, as a function of R, obtained for $\alpha = 1.303$ and $\gamma = 2.280$.

We have performed an (α, γ) dependence analysis of these static properties: R_{sn} is found by solving a third order equation derived from the conditions for the existence of more than one fixed point; and R_{Hf} is obtained through the linear stability analysis of the upper branch solution. The saddle node bifurcation takes place for any pair (α, γ) satisfying condition (1). Figure 3 displays the parameter
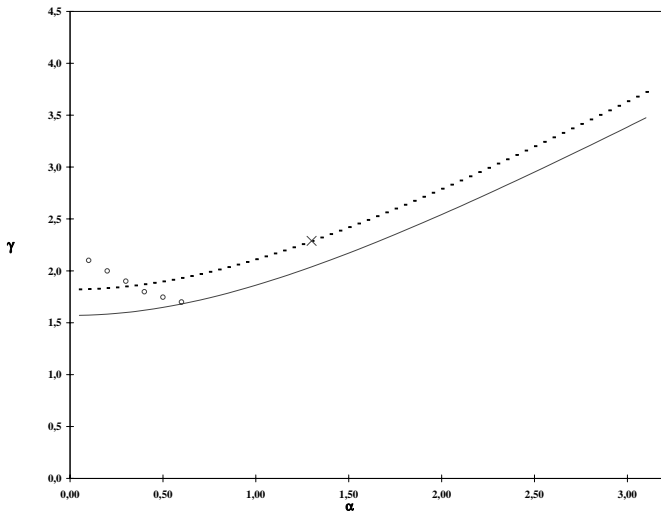
Fig. 3. Main dynamical properties in the parameter space (α, γ). Condition (1) is satisfied above the solid line. The dotted line is the locus of the minimum R_{sn} for each α, on which the cross indicates the locus of the smallest R_{sn}. Below the circled-line the upper branch is always stable and no Hopf bifurcation occurs.

space with: the bounding curve corresponding to condition (1), the locus of the smallest R_{sn} when either α or γ is fixed; the pair $(\alpha = 1.303, \gamma = 2.280)$ for which R_{sn} is minimal; and the line of double-zero co-dimension-two bifurcations, where the saddle node and the Hopf bifurcation occur at the same critical Reynolds number. Below this line, the upper branch fixed point is stable at the saddle node bifurcation and no Hopf bifurcation occurs. Above this line, the Hopf bifurcation criticality is given by the sign of the third order term coefficient in its radius expansion. This coefficient can be derived from the original dynamical system through a rather long but straightforward calculation, and remains positive for the range of parameters (α, γ), that we consider. The bifurcation is thus subcritical in this range of parameters. Altogether the pair $(\alpha = 1.303, \gamma = 2.280)$ appears as a generic set, which is of value, for studying the dynamics.

In conclusion, there are only two types of bifurcation diagram. Either the upper branch solution is stable at the saddle node bifurcation and the phase space dynamics reduces itself to that of a simple bistable system with a single separatrix made of the stable manifold of the only unstable state. This is the kind of system described in [12]. Or the upper branch solution is unstable at the saddle node bifurcation and stabilizes at a higher Reynolds number through a subcritical Hopf bifurcation leading to the coexistence of an unstable limit cycle with the unstable lower branch solution. One then expects a more complex dynamics, which we investigate now on the basis of a phase space simulation for the parameters $(\alpha = 1.303, \gamma = 2.280)$.

3 Phase space simulation

In order to make maximum benefit from the simulation, one needs a representation of the trajectories of the dynamics, and not only the evolution of some arbitrarily

chosen quantity such as the perturbation energy. In the present case, we take advantage of the phase space structure. When R is larger then R_{sn}, there are three fixed points which define a plane in four-dimensional space. An arbitrary normal direction is chosen to define a three-dimensional visualization space. The dynamics is then orthogonally projected onto this space. An interesting advantage of this visualization space is that it follows the fixed points and thus naturally adapts to their changing positions when varying the Reynolds number. Also, we have not noticed any significant influence of the arbitrarily chosen normal direction used to construct the visualization space. Figure 4a and 4b display the characteristics of the dynamics, for $R_{sn} < R < R_{Hf}$ and $R > R_{Hf}$, respectively. The three fixed points are labeled (BS) for the basic state, (LB) for the lower branch and (UB) for the upper branch. The basic state is conventionally set at the origin. One observes that, in agreement with the eigenvalue picture described above, the asymptotic dynamics concentrates on a bidimensional manifold.

For $R_{sn} < R < R_{Hf}$, (Fig 4a), we have chosen four kinds of initial conditions. Trajectories (1) and (2) start close to the lower branch fixed point but "on the side" of the basic state. Trajectories (3) and (4) also start close to the lower branch fixed point but "on the other side". Trajectories (5), (6) and (7) start in the middle of nowhere. Trajectory (8) starts close to and moves away from the unstable upper branch fixed point. All trajectories obviously relax to the basic state, the only stable fixed point. But there are two kinds of trajectories, those such as (1) and (2) relaxing in a rather direct way and the others exhibiting cyclic transients before relaxing. These transients are not only observed when initial conditions are chosen close to the upper branch fixed point such as for trajectory (8), but actually as soon as the initial conditions are on the "wrong side" of the lower branch fixed point (see trajectories (3) and (4)).

For $R > R_{Hf}$, (Fig 4b), we have chosen three kinds of initial conditions. Initial conditions (1) to (5) are essentially chosen along the same direction, at an increasing distance from the basic state. One can see that the unstable spiral has turned into a stable one and accordingly that a third kind of trajectory has emerged, those asymptotically ending on the newly stable fixed point. More precisely, trajectories (1) to (4) end at the basic state, immediately (1, 2) or after a long transient (3, 4), and trajectory (5) ends at the stable upper branch fixed point. One already surmises that the future of a trajectory is strongly related to its "landing point" on the bidimensional inertial manifold. This is better illustrated following trajectories (6) and (7). Their initial conditions are very close to one another, but trajectory (6) relaxes to the basic state after a long cyclic transient, whereas trajectory (7) tends towards the other stable fixed point. The two trajectories remain very close until they reach the bidimensional manifold on which they diverge from each other. This behavior illustrates the complexity of the separatrix shape, leading to a strong dependence on the initial conditions, without the need for any chaotic behavior.
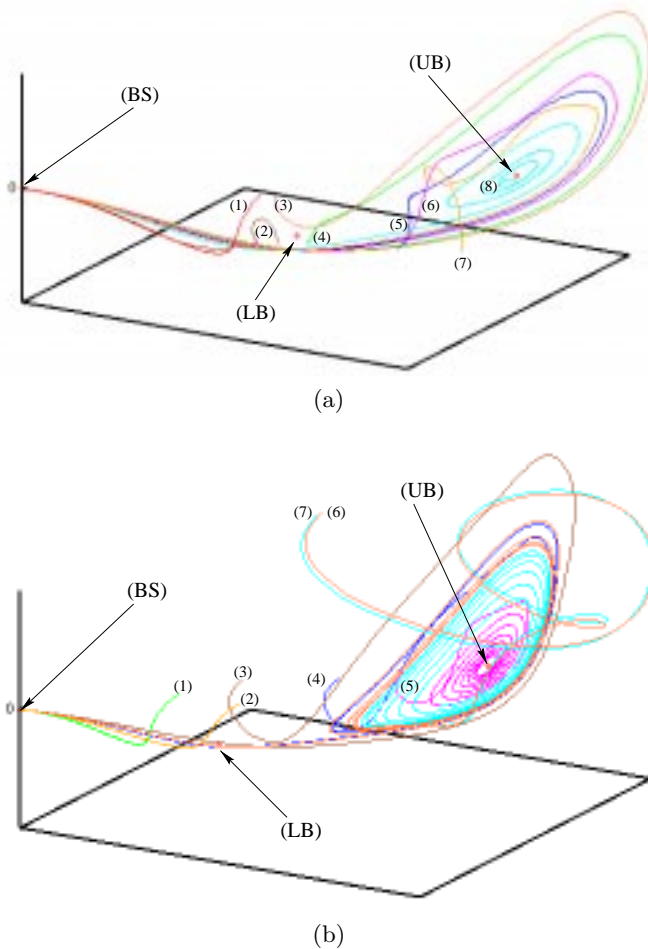
(a)

(b)

Fig. 4. Trajectories in the visualization space for (a) $R = 120$ and (b) $R = 160$.

To search for the actual stability boundaries one needs to characterize the attraction basins of the various stable states. Since a complete exact description of the separatrix can not be achieved, we concentrate on a statistical level of description. Anticipating further comparison with experimental studies, we imagine a finite amplitude perturbation of the basic state, and statistically study the response of the system. Introducing a specific perturbation involves choosing a special initial condition in phase space. In practice, we model the selection of the perturbation "shape" by the choice of a directing vector, and the perturbation amplitude A by the distance between the initial condition and the basic state. Then a thousand trajectories are computed, starting from initial conditions randomly chosen around the desired perturbation. These follow a Gaussian distribution, such as one would expect in an experimental context. The probability p_1 to reach the upper branch fixed point is most easily obtained by counting the trajectories asymptotically converging towards this point. Among the trajectories relaxing towards the basic state, a long transient refers to "turning around the upper branch", at least once. The probabilities p_2 to exhibit long transients before relaxing, and p_3 to relax directly to the basic state, are then easily extracted by simple counting.
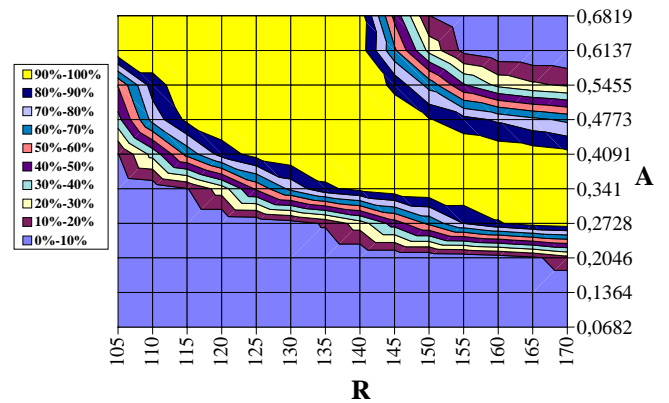

Fig. 5. Probability p_2 of trajectories exhibiting transients depending on R and the perturbation amplitude.

Figure 5 displays p_2 dependence on the perturbation amplitude and the Reynolds number. Three regions appear. In the upper right corner, where p_2 decreases to zero, we also have $p_3 = 0$, and so almost all initial conditions reach the upper branch fixed point. In the lower left corner, p_2 also decreases to zero, but this time $p_1 = 0$ and almost all initial conditions relax directly to the basic state. Then in the center, there is a large region, where almost all trajectories exhibit long transients before relaxing. These three regions in the (R, A) space are separated by rather wide bands where there is a competition between two of the three possible dynamics, namely between the direct relaxation and the long transients in the lower band and between long transients and convergence to the upper branch fixed point in the upper band. These areas of competition between two different kinds of dynamics reflect the separation between the initial conditions, operated by the stable manifold of the unstable solutions, respectively the unstable fixed point for the lower band and the unstable limit cycle for the upper band.

Studying supercritical bifurcations in extended systems, one often draws the bifurcation diagram by plotting the amplitude of the most unstable mode as a function of the control parameter. For a subcritical transition, no well-defined mode can be identified and one needs to find a convenient measure of the "distance" to the basic state. Whereas this distance is easily found in a model as simple as the one studied here, it is rarely the case in an experimental context. This is why an interesting feature of Figure 5, obtained through the statistical procedure described above, is its qualitatively good description of the unstable branches of the underlying bifurcation diagram (see Fig. 2).

4 Discussion

In the introduction, various essential features of the subcritical transition to turbulence have been briefly described. In this section we attempt to make a connection between the outputs of the present study and those features.

As already stated, the Waleffe's model has been derived from the Navier-Stokes equations in the case of a

velocity profile sharing the stability property of the plane Couette profile. Hence the subcriticality is automatically obtained. The spatio-temporal intermittency is not supposed to be described by a purely temporal system obtained by projecting the dynamics on a set of Galerkin modes. Still, it is worth underlining the similarity between those modes and the finite amplitude structures experimentally [6,15] or numerically [7–9,16] observed, both being made of streamwise vortices and streaks, both being unstable.

The other features of the transition deal with the temporal evolution of a disturbance. Experimentally, a nonlinear response to finite amplitude perturbation can be obtained by triggering the plane Couette flow with an instantaneous localized transverse jet and monitoring the disturbance evolution. In a recent work, Bottin, Daviaud, Manneville and Dauchot [4] studied the case of very large amplitude perturbations. For $R < R_u$, the disturbance relaxes almost instantaneously, for $R > R_u$ it initiates a turbulent spot, transient when $R < R_c$ and sustained when $R > R_c$. For the purpose of clarity, let us emphasize that the notations R_c and R_g actually describe the same threshold. Here we chose to use R_g, following the conceptual context of global subcriticality introduced in [12]. The Chaté and Bottin study [5] together with more recent results, complete this picture for lower perturbation amplitudes. For $R_u < R < R_g$, long-lived transients are not always observed and rapid relaxation may occur as well. Similarly for $R > R_g$, the sustained regime is not the only asymptotic regime; transients and even rapid relaxations are also observed. Clearly, the localized perturbation shape and amplitude strongly condition the disturbance evolution. Unfortunately, the knowledge of the "efficiency" and "relevance" of a perturbation is *a priori* a hard problem linked to the poor knowledge of the phase space, especially in the hydrodynamics context. Also, the perturbation is certainly not perfectly monitored and, as emphasized in [5], only a statistical study of the response can be conducted. In their study Bottin and Chaté performed a series of experiments by locally perturbing the laminar flow, either at fixed Reynolds number and varying the amplitude of perturbation, or the converse. They estimated the percentage p to reach the sustained turbulent regime and determined the location of the $p = 1/2$ curve in the (R, A) parameter space. The turbulent spot is considered as sustained when its lifetime is longer than an upper cutoff $t_{max} = 300$ s. Here, on the basis of a compilation of Bottin and Chaté's data together with some new set of data, we define an inferior cutoff $t_{min} = 10$ s, such that disturbances with a lifetime shorter than t_{min} are considered as relaxing without being transient. Figure 6 displays two amplitude curves. Below the bulleted curve, more than 95% of the perturbations relax immediately. Above the diamond curve, more than 95% of the perturbations turn into a sustained turbulent spot. One observes a picture very similar to that of Figure 5, with three domains in the (A, R) space, one dominated by sustained turbulent spots, one by transients and one by immediate relaxations. Those domain shapes clearly call for an identification of R_u with R_{sn} and R_g with R_{Hf}. The present statistical de-
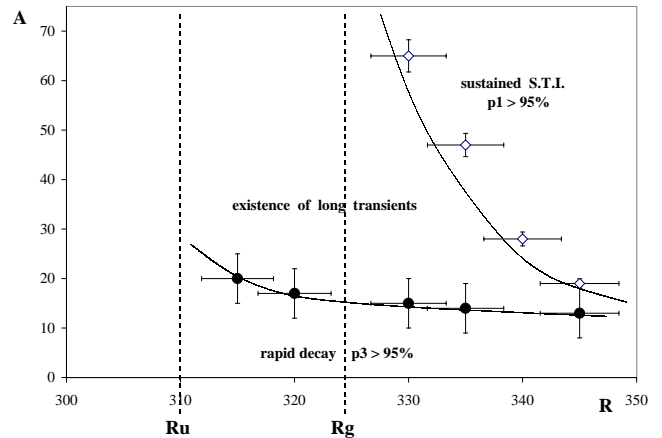

Fig. 6. Critical amplitude curves separating the three different dynamics (see text for details).

scription thus allows us to give a simple interpretation to the thresholds observed experimentally, whereas a direct comparison of Figure 6 with the bifurcation diagram of Figure 2 would have been quite hazardous.

Altogether, Waleffe's model shows at a global level, the now widely accepted picture of the transition to turbulence in plane Couette flow. On increasing the Reynolds number, a saddle node bifurcation at $R = R_u$ gives rise to unstable stationary states. These states and their stable manifolds progressively draw the phase space structure and induce longer and longer transients which lead to a regime of metastable spatio-temporal intermittency. At $R = R_g$, this spatio-temporal intermittent repulsor turns into an attractor leading to the sustained spatio-temporal intermittent regime.

References

1. F. Waleffe, Phys. Fluids **9**, 883-900 (1997).
2. O. Dauchot, F. Daviaud, Phys. Fluids **7**, 335-343 (1992).
3. F. Daviaud, J. Hegseth, P. Bergé, Phys. Rev. Lett. **69**, 2511-2514 (1992).
4. S. Bottin, F. Daviaud, P. Manneville, O. Dauchot, Europhys. Lett. **43**, 171-176 (1998).
5. S. Bottin, H. Chaté, Eur. Phys. J. B **6**, 143-155 (1998).
6. S. Bottin, O. Dauchot, F. Daviaud, P. Manneville, Phys. Fluids **10**, 2597-2607 (1998).
7. N. Nagata, J. Fluid Mech. **217**, 519-527 (1990).
8. R.M. Clever, F.H. Busse, J. Fluid Mech. **234**, 511-527 (1992).
9. A. Cherhabili, U. Ehrenstein, J. Fluid Mech. **342**, 159-177 (1997) .
10. J.S. Baggett, L.N. Trefethen, Phys. Fluids **9**, 1043-1053 (1997).
11. F. Waleffe, Phys. Fluids **7**, 3060-3066 (1995).
12. O. Dauchot, P. Manneville, J. Phys. II France **7**, 371-389 (1997).
13. A. Schmiegel, B. Eckhardt (preprint).
14. J.M. Hamilton, J. Kim, F. Waleffe, J. Fluid Mech. **287**, 317-348 (1995).
15. S. Bottin, O. Dauchot, F. Daviaud, Phys. Rev. Lett. **79**, 4377-4380 (1997).
16. D. Barley, L. Tuckerman (preprint).